MILAN M. MILOŠEVIĆ[1]
PETAR S. MATAVULJ[1]
GORAN Z. MASHANOVICH[2]

[1]Faculty of Electrical Engineering, University of Belgrade, Belgrade, Serbia

[2]Advanced Technology Institute, University of Surrey, Guildford, UK

SCIENTIFIC PAPER

621.372.8+546.28:621.371.3

SINGLE MODE AND POLARIZATION INDEPENDENCE IN THE STRAINED SILICON–ON–INSULATOR RIB WAVEGUIDES*

In this paper we investigate the most popular silicon waveguide structures in the form of a silicon–on–insulator (SOI) rib waveguide. Single mode and birefringence free conditions in these relatively small waveguides are discussed and the influence of the top oxide cladding stress is analyzed. Field profiles for a wide range of waveguide cross section shapes and dimensions are systematically considered. Design guidelines for this type of SOI waveguides are presented.

In the last few years there has been increased interest in silicon photonic devices due to performance and cost reasons. Silicon–on–Insulator (SOI) platform has shown the ability to provide all ever increasing demands and became today the most popular choice for waveguide systems [1,2]. As SOI is extensively used in microelectronics industry, it is also one of the most promising materials for optical/electrical integration. After research activities in planar [3] and large rib waveguides [4] a lot effort has been placed into investigation of small compact devices and that's why both small cross sectional rib and strip waveguides were studied extensively [5,6]. Typical wavelengths for SOI applications are 1.3 μm and 1.55 μm, but longer wavelengths are not suitable (except in the 3–3.5 μm range) due to absorption spectra in silicon dioxide [7]. Highly desirable and complex devices such as Bragg gratings [8], optical modulators [9] and light sources [10] prove that this is an ideal time to be working on silicon photonics.

In an SOI waveguide, light is guided in a silicon core separated from the silicon substrate by a buried SiO_2 layer (BOX) acting as the lower cladding. High index contrast between the cladding and waveguide core facilitates the optical confinement and guiding of light. Large rib waveguides have been studied by a number of researchers [11–14] to find single mode behavior and low loss propagation. Soref et al. [15] first proposed a simple equation to describe the monomodal condition of these waveguides:

$$\frac{W}{H} \le 0.3 + \frac{r}{\sqrt{1-r^2}}\ , \quad (\text{for } 0.5 \le \mathrm{r} < 1)\,, \tag{1}$$

where r is the ratio of slab height to overall rib height, and W/H is the ratio of waveguide width to overall rib height. Their analysis of the waveguides was limited to shallow etched ribs ($r > 0.5$) and the waveguide dimensions were assumed to be larger than the operating wavelength. Chan et. al. [5] proposed the design guidelines for small rib waveguides ($0 < \mathrm{r} < 0.5$ and $1.0 < \mathrm{H} < 1.5$ μm), but only with air top cladding:

$$\frac{W}{H} \le 0.05 + \frac{(0.94 + 0.25\,H)\,r}{\sqrt{1-r^2}}\,, \tag{2}$$

$$D_{\min} = 0.06 \times 10^{-6} + 0.556\,H. \tag{3}$$

Equation (2) defines the quasi–TM single mode boundary, and hence provides guidance on the geometric limitations to retain single mode behavior, whilst equation (3) defines the minimum etch depth $D_{\min}$ required to obtain polarization independence. The influence of the top oxide cover on waveguide birefringence has been analysed for larger rib waveguides with height of 2.2 μm [16].

This paper reports on simulations for relatively small cross sectional rib waveguides. The influence of top oxide cladding stress on waveguide birefringence and single mode behaviour is systematically presented. Field profiles for a wide range of waveguide cross section shapes and dimensions are given. We were primarily interested in fundamental mode and first higher order mode to define the boundary between single mode and multimode behaviour. It is also described the influence of waveguide sidewall angle to the optical mode confinement.

The paper is organized as follows. In the first section, the stress theory and its influence to the total birefringence is presented. Then, calculation of field profiels and single mode behavior is explained, and the concluding remarks are summarized in the last section.

*Paper presented at the "Šesti seminar mladih istraživača" (6th Seminar of Young Researchers), Belgrade, December 24–26, 2007.

Author address: M. Milošević, Sinđelićeva 135, 35210 Svilajnac, Serbia
E–mail: milance24@gmail.com
Paper received: December 24, 2007.
Paper accepted: February 6, 2007.

STRAIN THEORY AND MODAL WAVEGUIDE BIREFRINGENCE

The cross section view of analyzed rib waveguide is shown in Figure 1. Stress in the upper SiO_2 layer produces a stress distribution within and near the Si rib, which in turn causes a change of the refractive index in both materials due to the photoelastic effect. We assume that the thickness of the upper cladding film on the rib sidewalls is 70% of that on the top to simulate the film deposition used in experiments. Simulations were performed at an operating wavelength of λ = 1.55 μm, while the waveguide height was kept constant and was equal H = 1.35 μm. We assumed waveguide sidewalls to be vertical ($\theta = 90^o$) except it is said contrary.

Modal waveguide birefringence is defined here as the difference between the effective indexes of the two orthogonally polarized modes, horizontally polarized mode (quasi–TE) and vertically polarized mode (quasi–TM) $\Delta N_{eff} = N_{eff}^{TE} - N_{eff}^{TM}$. To achieve zero–birefringence, an optimisation of rib waveguide dimensions is necessary [17]. The total birefringence is, however, the sum of the geometrical birefringence (ΔN_{geo}) and stress induced birefringence (ΔN_{stress}) [18]: $\Delta N_{\text{eff}} = \Delta N_{geo} + \Delta N_{stress}$. The stress induced birefringence can be expressed as:

$$\Delta N_x = N_x - N_0 = -C_1\sigma_x - C_2(\sigma_y + \sigma_z)$$
$$\Delta N_y = N_y - N_0 = -C_1\sigma_y - C_2(\sigma_x + \sigma_z) \quad (4)$$

Here, σ_x, σ_y and σ_z are the principal components of the relative stress tensor, N_x and N_y are the components of the material's refractive index, N_0 is the refractive index without stress, and C_1 and C_2 are the stress–optic constants related to the Young's modulus (E), Poisson's ratio (ν), and the photoelastic tensor elements (p_{11} and p_{12}) as:

$$C_1 = \frac{N^3}{2E}(p_{11} - 2\nu p_{12})$$
$$C_2 = \frac{N^3}{2E}(-\nu p_{11} + (1-\nu)p_{12}). \quad (5)$$

One source of birefringence, however, is strain due to the temperature difference before and after manufacturing processes (between the operating temperature T_0 and the reference temperature T_{ref}, $\Delta T = T_0 - T_{ref}$). The stress and strain are related as follows:

$$\begin{bmatrix}\varepsilon_x\\ \varepsilon_y\\ \varepsilon_z\end{bmatrix} = \frac{1}{E}\begin{bmatrix}1 & -\nu & -\nu\\ -\nu & 1 & -\nu\\ -\nu & -\nu & 1\end{bmatrix}\begin{bmatrix}\sigma_x\\ \sigma_y\\ \sigma_z\end{bmatrix} + \alpha\Delta T \cdot I, \quad (6)$$

where ε_x, ε_y, and ε_z are the principal strain components along the x, y and z direction, respectively, α is thermal expansion coefficient and I is the unit vector. As it can be seen from (6) the stress consists of the photoelastic strain and thermal induced strain. By inverting (6) the stress distribution can be obtained and further, according to (4) the material refractive index distribution. Now, we can solve Maxwell's equations and obtain the effective mode indexes for both quasi–TE and quasi–TM modes [17].

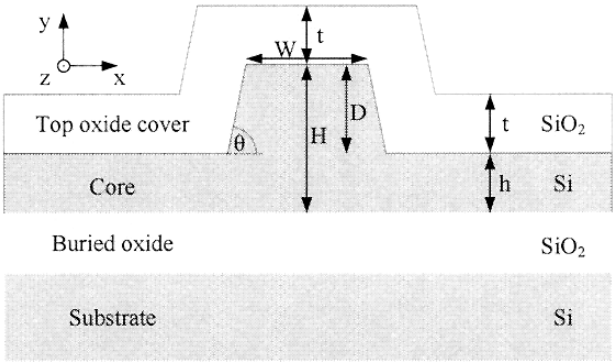

Figure 1. The cross section of an SOI rib waveguide (t is the top oxide layer thickness, H is rib height, D (D = H – h) is etch depth, W is waveguide rib width and θ is sidewall angle).

Table 1. Material parameters used in the calculations for wavelength of 1550 nm

Material	Si	SiO_2
p_{11}	–0.101	0.16
p_{12}	0.0094	0.27
Youngs Modulus, E (GPa)	130	76.7
Poisson's ratio, ν	0.27	0.186
Thermal expansion coefficient, α ($\times 10^{-6}$ K^{-1})	3.6	0.54

Table 1 summarizes all material parameters used in numerical computations. The difference between the operating and reference temperature is assumed to be ΔT = –980 K. Figure 2 shows the simulated stress distribution in x and y direction of waveguide cross section. Computation window size for stress calculation is set to be 100 μm×100 μm, large–wide enough that the edge effects do not distort the stress distribution in the vicinity of the ridge waveguide. This provides good enough accuracy and calculation time. Simulations were performed by the finite element method (FEM) on a nonuniform mesh of triangular elements [17]. At the waveguide center, we get $\sigma_x \approx$ –60 MPa, $\sigma_y \approx$ 120 MPa, while for SiO_2 upper and lower cladding $\sigma_{film} \approx$ –290 MPa (σ_{film} represents the in–plane stress component in the uniform film far enough from the ridge). The primarily in–plane (x) stress in the oxide film compresses Si ridge resulting in a compressive strain in the x direction and higher tensile strain in the y direction. This anisotropy is the main reason for stress–induced birefringence.

Figure 3 represents the influence of waveguide parameters to the modal waveguide birefringence. The effective indexes for both quasi–TE and quasi–TM modes and their difference were calcula-

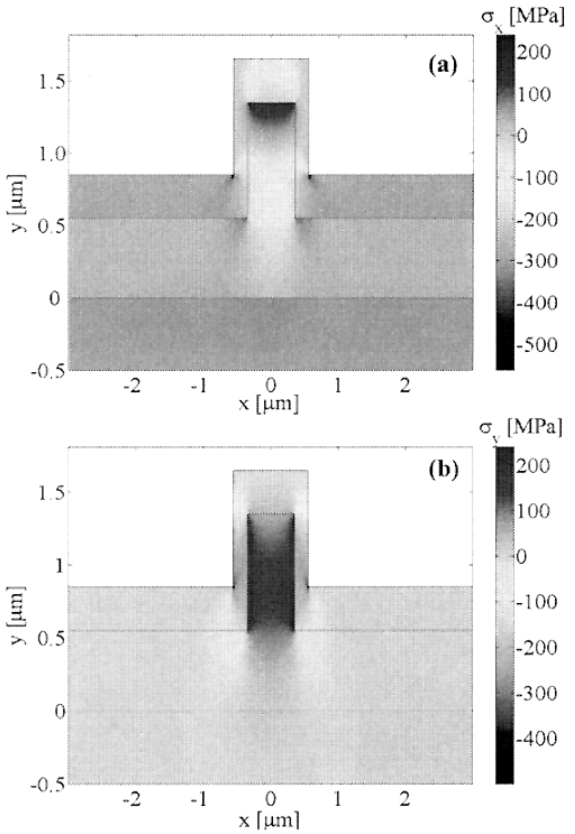

Figure 2. Stress field distribution (a) in the x direction, σ_x and (b) in the y direction, σ_y.

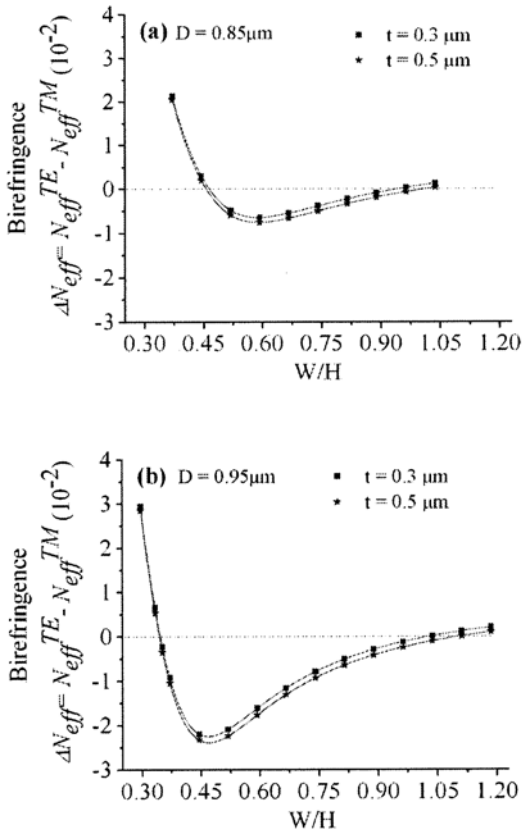

Figure 3. Modal waveguide birefringence as a function of waveguide parameters and upper oxide cladding thickness for waveguide etch depth of (a) D = 0.85μm and (b) D = 0.95μm. (H = 1.35 μm, λ = 1.55 μm, and θ = 90°).

ted while keeping the waveguide height and etch depth constant during the simulations. Once again, we assumed an operating wavelength of $\lambda = 1.55$ μm and vertical waveguide sidewalls. For a certain value of top oxide cover thickness a series of points for modal birefringence were evaluated for a number of waveguide rib width values. It can be remarked that for a certain D and t, two zero birefringence points exists. In both cases, for a certain value of etch depth, curves are more separated when waveguide rib width increases. Increase in upper oxide thickness shifts the ΔN_{eff} curve to down. If we compare the Figure 3a with Figure 3b, it can be noticed that lower value of etch depth for a certain t shifts up the curves. We can conclude that only a certain values of etch depth will provide birefringence free operation and that the carefull design of waveguide parameters need to be imposed during the fabrication to match the polarization independence.

SINGLE MODE CONDITION (SMC)

Besides polarization independence, an interesting research topic in silicon photonics is to find appropriate waveguide parameters that will satisfy single mode operation. Simulations were performed by the FEM method because it can easy incorporate the change in material effective index caused by the upper oxide layer via photoelastic effect. Two cases were studied, one represents the waveguide with an air cover, and other is the waveguide with an oxide cover of 0.3 μm in thickness. Like in previous case, for a certain value of waveguide parameters we calculated the field profiles for both quasi–TM and quasi–TE modes.

Figure 4 represents the influence of waveguide dimensions to the quasi–TM mode shape. We calculated the fundamental quasi–TM mode and first higher order mode. Simulations were performed for vertical waveguide sidewalls ($\theta = 90^o$) and different values of waveguide etch depth and rib width are taken into account. Narrower waveguide rib width will squeeze the mode towards the center (Figure 4a, b, d, e), but in the case for quasi–TM_{10} (Figure 4f) mode is totally placed off center and we can expect to vanish in the waveguide during the wave propagation.

Figure 5 shows the influence of waveguide sidewalls to the quasi–TE mode shape for a certain waveguide rib width and etch depth. In all cases energy density is concentrated in the core region and decays rapidly in the top oxide cladding and buried oxide region, similarly to Figure 4. We assumed slan-

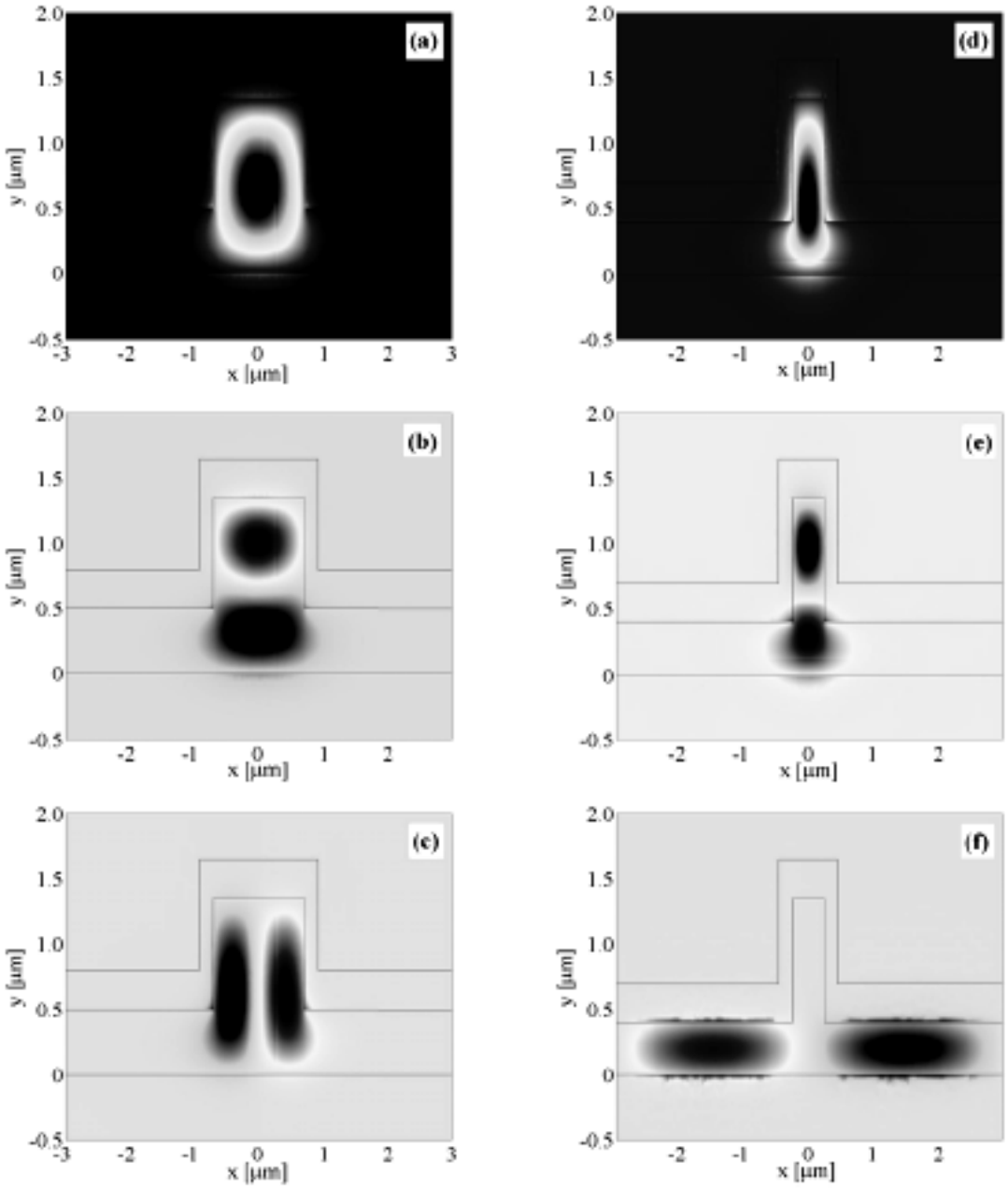

Figure 4. Field profiles for fundamental and first higher order quasi–TM mode. (Left panel). D = 0.85 μm, W = 1.4 μm. (a) quasi–TM_{00}, (b) quasi–TM_{01}, and (c) quasi–TM_{10}. (Right panel) D = 0.95 μm, W = 0.5 μm. (d) quasi–TM_{00}, (e) quasi–TM_{01}, and (f) quasi–TM_{10}.

ted waveguide sidewalls of 80° because of previous experiments based on rib waveguides. It can be remarked that the field is much concentrated to the core center when waveguide sidewalls are slanted. Field is much stronger and one can not expect that higher order modes will vanish during the propagation through the waveguide.

Figure 6 represents the single mode conditions for both quasi–TE and quasi–TM modes. We focused one specific value of waveguide etch depth and change waveguide rib width until first higher order mode was found. This was done for a waveguide with an upper oxide layer of 0.3 μm in thickness and for a waveguide with an air top cladding. In both cases we assumed vertical waveguide sidewalls. The case without top cover corresponds to the isotropic case. Here, we found great difference compared to the anisotropic case. Deeper etch depths provide that the points calculated with including stress effects are below the points calculated in isotropic case. This difference is greater in the case for quasi–TM mode (Figure 6b) than in the case for quasi–TE mode (Fi-

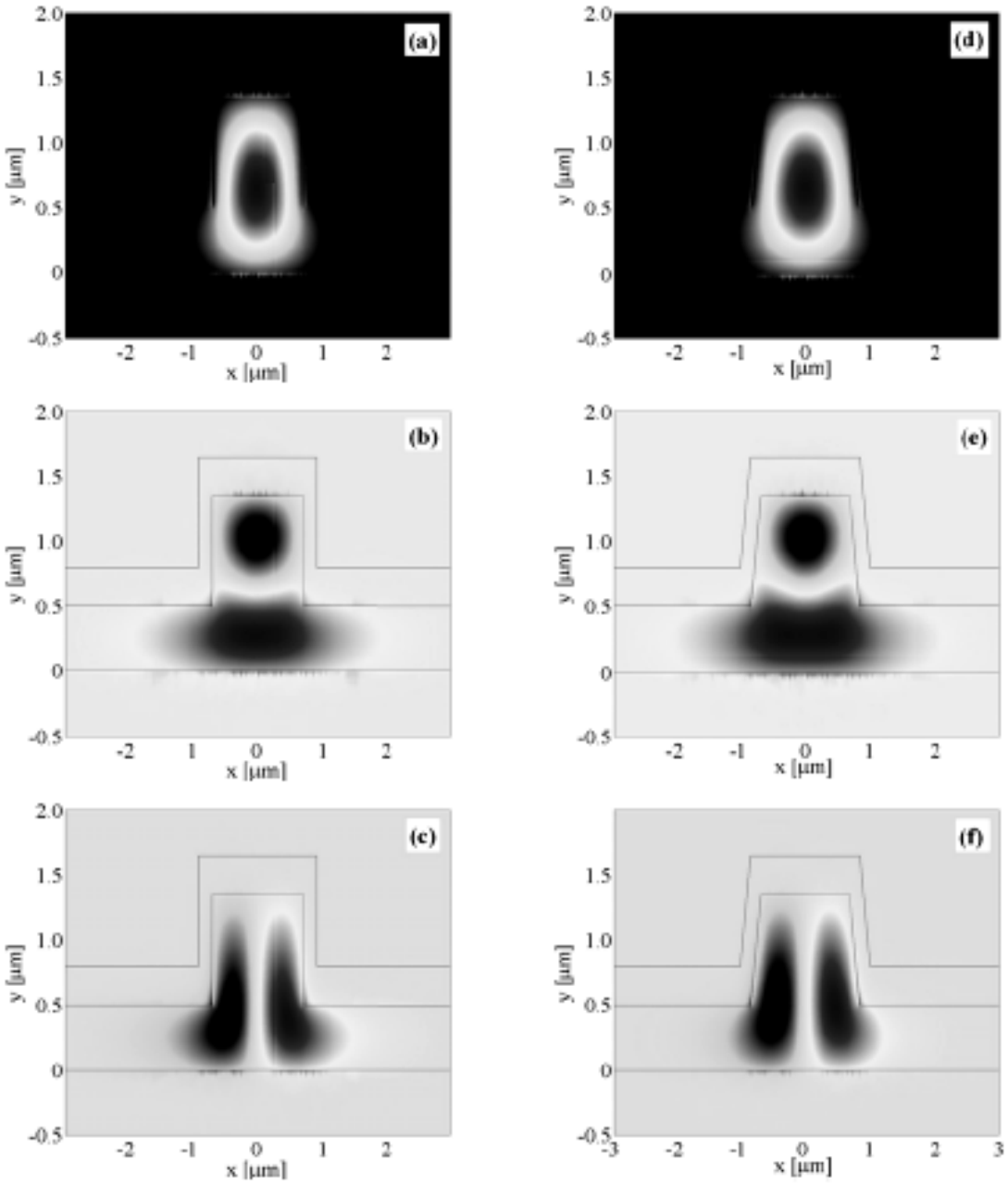

Figure 5. Field profiles for fundamental and first higher order quasi–TE mode. (Left panel). Vertiacal sidewalls, θ = 90°; (a) quasi–TE_{00}, (b) quasi–TE_{01}, and (c) quasi–TE_{10}. (Right panel) Slanted sidewalls, θ = 80°; (d) quasi–TE_{00}, (e) quasi–TE_{01}, and (f) quasi–TE_{10} (in both cases D = 0.85 μm, W = 1.4 μm).

gure 6a). We can conclude that the both curves have higher slope when stress effects are taken into account. Like in the isotropic case, single mode quasi–TM curve is more important because it sets the total boundary between single mode and multimode behavior.

CONCLUSION

Silicon photonics opens great opportunities for wide range of applications in integrated optics, telecommunications, data analysis, sensors applications and imaging. Rib waveguide represents the basic building component of such systems. In this paper we systematically discussed about stress engineering tools in order to provide polarization independence and single mode operation. We discussed about top oxide cover and waveguide sidewall influence to total birefringence and single mode condition. Field profiles for a large variety of waveguide cross sections and waveguide dimensions were presented. Appropriate design guidelines that will provide desirable demands are explained and described.

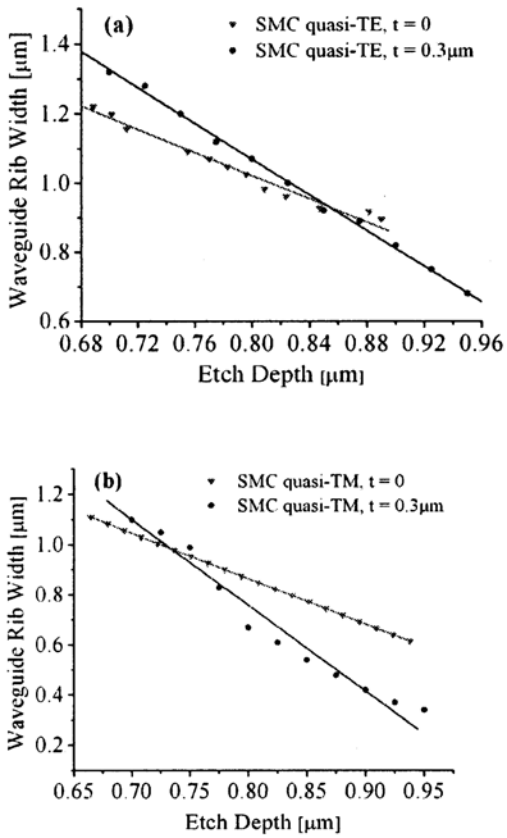

Figure 6. Single mode conditions as a function of waveguide rib width, etch depth and top oxide cover thickness for (a) quasi–TE mode and (b) quasi–TM mode. (H = 1.35 μm, λ = 1.55 μm, and $\theta = 90^{o}$).

REFERENCES

[1] E. Cortesi, F. Namavar, R.A. Soref, Proc. IEEE SOS/SOI Tech. Conf. (Cat. No. 89CH2796–1), 1989, pp. 109.

[2] B.N. Kurdi, D.G. Hall, Opt. Lett. **13** (2) (1988) 175–177.

[3] A. Rickman, G.T. Reed, B.L. Weiss, F. Namavar, IEEE Photon. Tech. Lett. **4** (6) (1992) 633–635.

[4] J. Schmidtchen, A. Splett, B. Schuppert, K. Petermann, Proc. IEEE International SOI Conf. (Cat. No.91CH3053–6), 1991, pp. 142–143.

[5] S.P. Chan, C.E. Png, S.T. Lim, V.M.N. Passaro, G.T. Reed, J. Lightwave Tech. **23** (6) (2005) 1573–1582.

[6] K. Yamada, H. Fukuda, T. Watanabe, T. Tsuchizawa, T. Shoji, S.–I. Itabashi, Proc. LEOS 2nd Group IV Photonics, 2005, pp. 186–188.

[7] R.A. Soref, S.J. Emelett, W.R. Buchwald, J. Opt. A: Pure Appl. Opt., **8** (10) (2006) 840–848.

[8] S.P. Chan, V.M.N. Passaro, S.T. Lim, C.E. Png, G.T. Reed, Proc. SPIE, 5248 (2003) 273–283.

[9] C.E. Png, S.P. Chan, S.T. Lim, G.T. Reed, J. Lightwave Technol. **22** (6) (2004) 1573–1582.

[10] O. Boyraz, B. Jalali, Opt. Express **12** (2004) 5269–5273.

[11] S.P. Pogossian, L. Vescan, A. Vonsovici, J. Lightwave Technol. **16** (1998) 1851–1853.

[12] O. Powell, J. Lightwave Technol. **20** (2002) 1851–1855.

[13] L. Vivien, S. Laval, B. Dumont, S. Lardenois, A. Koster, E. Cassan, Opt. Commun. **210** (2002) 43–49.

[14] J. Lousteau, D. Furniss, A. Seddon, T. M. Benson, A. Vukovic, and P. Sewell, J. Lightwave Technol., **22** (2004) 1923–1929.

[15] R.A. Soref, J. Schmidtchen and K. Petermann, IEEE J. Quantum Electron., **27** (1991) 1971–1974.

[16] W.N. Ye, D.–X. Xu, S. Janz, P. Cheben, M.–J. Picard, B. Lamontagne, and N.G. Tarr, J. Lightwave Technol., **23** (2005) 1308–1318.

[17] M.M. Milošević, P.S. Matavulj, and G.Z. Mashanovich, Proc. 15th Telecom. Forum TELFOR, (2007) 401–404.

[18] S. Stanković, M. Milošević, B. Timotijević, P.Y. Yang, E.J. Teo, J. Crnjanski, P. Matavulj, and G.Z. Mashanovich, Acta Phys. Polonica A, 112 **5** (2007) 1019–1024.

IZVOD

JEDNOMODNO PROSTIRANJE I POLARIZACIONA NEZAVISNOST U SILICIJUMSKIM RIB TALASOVODIMA

(Naučni rad)

Milan M. Milošević[1], Petar S. Matavulj[1], Goran Z. Mashanovich[2]
[1]Elektrotehnički fakultet, Univerzitet u Beogradu, Srbija
[2]Advanced Technology Institute, University of Surrey, Guildford, UK

U ovom radu su prezentovane strukture trenutno vrlo popularnih silicijumskih rib talasovoda. Proučavan je uslov jednomodnog prostiranja i postizanja nultog dvojnog prelamanja sa razmatranjem uticaja naprezanja usled nanošenja tankog sloja oksida na jezgro talasovoda. Sistematično su analizirani profili polja za široki spektar dimenzija i poprečnih preseka talasovoda, i prikazana su odgovarajuća pravila dizajna ovakvih struktura.

Ključne reči: Polarizaciona nezavisnost • Silicijumska fotonika • Jednomodno prostiranje • Naprezanje •

Key words: Polarization independence • Silicon photonics • Single mode • Strain •